Heating of Chromospheres and Coronae. P. Ulmschneider, Space Solar Physics, Summer School Orsay 1-13.9.97, J.C. Vial, K. Bocchialini, K. Boumier eds. (1997) submitted

Heating of Chromospheres and Coronae

Peter Ulmschneider

Institut für Theoretische Astrophysik der Universität Heidelberg, Tiergartenstr. 15, D–69121 Heidelberg, Germany
ulmschneider@ita.uni-heidelberg.de

Abstract. Chromospheres and coronae owe their existence to mechanical heating. In the present work the mechanisms which are thought to provide steady mechanical heating are reviewed. These mechanisms can be classified as *hydrodynamical*– and *magnetic heating mechanisms* and each of these can be subdivided further on basis of the fluctuation frequency. Rapid fluctuations generated by the turbulence in the convection zones lead to acoustic waves and to mhd waves (AC–mechanisms), slow fluctuations to pulsational waves and to stressed fields with current sheets (DC–mechanisms).

Solar and stellar observations, as well as acoustic and mhd wave generation rate computations on basis of convection zone models and a Kolmogorov-type energy spectrum representation for the turbulence, provide great progress towards the understanding of the complete dependence of the chromospheres and coronae on the properties of the underlying stars.

1 Chromospheres and coronae

Chromospheres and coronae are hot outer layers of stars where the temperatures are much higher than the stellar effective temperature T_{eff}. In the chromospheres the temperatures rise in outward direction to values of around 10000 K, while in the coronae the temperatures are in the million degree range. These layers are observed in the Radio, UV and X-ray spectral ranges. That the Sun has a million degree corona was first discovered by Grotrian in 1939 and Edlén in 1941 by identifying the coronal lines (observed since 1869) as transitions from low lying metastable levels of the ground configuration of highly ionized metals. The green coronal line at 5303 Å for instance emanates from the ion FeXIV and the red line at 6374 Å from FeX. Observing the Sun in the UV from 300 to 1400 Å the OSO satellites in the 1960's then showed the full sequence of ions e.g. from OII to OVI, the latter emitted at a temperature of about 10^5 K, as well as MgX which indicates 10^6 K. The Lyman, Carbon and Silicon continua from these observations were later used to construct models (like by Vernazza, Avrett & Loeser 1981) of the outer solar atmosphere. The IUE and Einstein satellites in the 1970's and 1980's, measuring UV and X-ray emissions from stars, subsequently showed that the Sun is not exceptional, but that probably all nondegenerate stars have such hot outer shells.

Einstein observations (Vaiana et al. 1981) showed that *O- and B- stars*, which do not have surface convection zones, have strong X-ray emission which today is attributed not to contiguous layers around those stars, but to shocks generated by rapidly moving individual gas blobs driven by radiative instability (see Sec. 5 below) in the outer stellar envelope.

F-, G-, K- and M-stars have chromospheres and often coronae much like our Sun. These are attributed to the wave- and magnetic energy generation in the surface convection zones of these stars. Late giants and supergiants do not have coronae (Linsky 1985). Finally, *A-stars* appear to have neither chromospheres nor coronae. There is a conspicuous X-ray gap for A-stars (Vaiana et al. 1981) and no UV-emission indicating an outwardly rising temperature. However, theoretically it can be argued that these stars still have a strong radiation field where photospheric motions can be initiated and thus acoustic disturbances produced. It is well known that by wave energy conservation even a very small disturbance, propagating over many density scale heights, will generate shock waves which lead to dissipation rates proportional to the pressure (or density) (Ulmschneider 1991). As the radiative cooling goes with the square of the density it is seen that eventually heating will overwhelm cooling, leading to hot outer layers. However, this might be so far away from the star that no appreciable emission is generated and thus observed. Thus, theoretically at least, A-stars should also have hot outer envelopes. This supports our above stated conclusion that very likely all nondegenerate stars have hot outer layers.

Chromospheres and coronae have another very important property which should never be overlooked. Except for T-Tau type stars, where the chromospheric emission results from mass-infall from accretion disks, the typical star with a chromosphere and corona does not receive energy from infinity. Thus the detailed physics of chromospheres and coronae is completely dependent on the underlying star. We are faced with the great challenge to understand the dependence of chromospheres and coronae on the stellar interior. For this reason, in the present review, not only the individual heating mechanisms are discussed but an attempt is made to relate heating and mechanical energy fluxes to the structure of the convection zone. One day we expect that a careful simulation of the surface convection zone of a given star will result in an accurate prediction of its chromosphere and corona.

2 Necessity of mechanical heating

Consider a gas element in the chromosphere. An amount of heat dQ (erg/cm^3) flowing into the element across its boundaries raises the entropy in the element by

$$dS = \frac{dQ}{\rho T} \quad , \tag{1}$$

where T is the temperature and ρ the density. As the entropy in the gas element (moving in a wind with velocity v) is conserved, one has in the laboratory (Euler) frame

$$\frac{\partial S}{\partial t} + v\frac{\partial S}{\partial z} = \left.\frac{dS}{dt}\right|_R + \left.\frac{dS}{dt}\right|_J + \left.\frac{dS}{dt}\right|_C + \left.\frac{dS}{dt}\right|_V + \left.\frac{dS}{dt}\right|_M \quad . \tag{2}$$

Here t is time and z is the height in a plane-parallel atmosphere. The first four terms on the right hand side stand for radiative, Joule, thermal conductive and viscous heating. We have added a term $dS/dt|_M$ which increases the entropy due to *mechanical heating*. Mechanical heating comprises all processes which convert nonradiative, nonconductive hydrodynamic or magnetic energy (henceforth called mechanical energy) flowing through the element into microscopic random thermal motion.

As the chromosphere exists on the Sun for billions of years, one usually (for an average model) can neglect the term $\frac{\partial S}{\partial t}$ in Eq. (2). With a solar wind mass loss rate of $\dot{M} = 10^{-14} M_\odot/y$ one can compute a wind flow speed

$$v = \frac{\dot{M}}{4\pi\rho R_\odot^2} = \frac{10^{-14} 2 \cdot 10^{33}}{3 \cdot 10^7 4\pi \left(7 \cdot 10^{10}\right)^2 \rho} \approx \frac{1.1 \cdot 10^{-11}}{\rho} \quad . \tag{3}$$

Typical flow velocities in the chromosphere from this formula on basis of the Vernazza et al. (1981) model C, henceforth called VAL81, are shown in Tab. 1. Because the wind velocity in the chromosphere and transition layer is small

z (km)	0	500	1000	1500	2100	2543
T (K)	6400	4200	5900	6400	10000	447000
ρ (g/cm^3)	$2.7 \cdot 10^{-7}$	$6.0 \cdot 10^{-9}$	$4 \cdot 10^{-11}$	$2.5 \cdot 10^{-12}$	$1.2 \cdot 10^{-13}$	$2.3 \cdot 10^{-15}$
c_S (cm/s)	$8.3 \cdot 10^5$	$6.7 \cdot 10^5$	$9 \cdot 10^5$	$8.3 \cdot 10^5$	$1.5 \cdot 10^6$	$1.0 \cdot 10^7$
v (cm/s)	$4.0 \cdot 10^{-5}$	$1.8 \cdot 10^{-3}$	0.27	4.3	90	$4.7 \cdot 10^3$

Table 1. Temperature T, density ρ, sound speed c_S and wind velocity v in the VAL81 model as a function of height z.

compared to the other characteristic velocity, the sound speed c_S (see Tab. 1), the entire left hand side of Eq. (2) can be neglected. Below we will show that $dS/dt|_J$, $dS/dt|_C$, $dS/dt|_V$ can also be neglected in the chromosphere (while $dS/dt|_C$ is important only in the transition layer and corona). In the chromosphere we thus find

$$\left.\frac{dS}{dt}\right|_R + \left.\frac{dS}{dt}\right|_M = 0 \quad . \tag{4}$$

Conclusion: *In stellar chromospheres the main energy balance is between radiation and mechanical heating.* For simplicity of the argument we now assume gray radiation. With the mean intensity J (erg/(cm^2 s sterad Hz)), the

frequency-integrated Planck function B (erg/(cm^2 s sterad Hz)) and the gray absorption coefficient $\overline{\kappa}$ (1/cm) one finds

$$\frac{4\pi\overline{\kappa}}{\rho T}(J - B) + \left.\frac{dS}{dt}\right|_M = 0 \quad . \tag{5}$$

In the special case of *radiative equilibrium* one has $dS/dt|_M = 0$ and obtains $J = B$. With $J = \sigma T_{eff}^4/2\pi$, valid for the surface of a star, roughly represented by a black body of effective temperature T_{eff} (the factor 1/2 comes from the fact that there is only radiation going away from the star), and $B = \sigma T^4/\pi$, one gets for the outer stellar layers a boundary temperature

$$T = \left(\frac{1}{2}\right)^{1/4} T_{eff} \approx 0.8\, T_{eff} \quad . \tag{6}$$

That is, in absence of mechanical heating we would expect that the regions above the stellar surface have temperatures of the order of the boundary temperature. However, as a chromosphere is a layer where the temperature rises in outward direction to values $T \gg T_{eff}$, it is clear that one must have $B \gg J$ and therefore $dS/dt|_M \gg 0$. This shows that for chromospheres mechanical heating is essential. In addition, as the energy loss of the transition layer and corona cannot be balanced by thermal conduction from a reservoir at infinity, but must ultimately be supplied from the stellar interior, we conclude that *for the existence of chromospheres and coronae mechanical heating is essential.*

Moreover, chromospheres and coronae can only be maintained if mechanical heating is supplied *constantly.* The time scale, in which an excess temperature will cool down to the boundary temperature if the mechanical heating were suddenly disrupted, is given by the the *radiative relaxation time* for which we have

$$t_{Rad} = \frac{\Delta E}{-\Phi_R} = \frac{\rho c_v \Delta T}{16\overline{\kappa}\sigma T^3 \Delta T} = \frac{\rho c_v}{16\overline{\kappa}\sigma T^3} \approx 1.1 \cdot 10^3\ s \quad . \tag{7}$$

Here we have expanded the radiative cooling rate $-\Phi_R = 4\overline{\kappa}\sigma(T^4 - T_{eff}^4/2) \approx 16\overline{\kappa}\sigma T^3 \Delta T$ for $T_{eff}^4/2 \approx T^4$ and at $z = 1280\ km$ in the VAL81 model, used temperature $T = 6200\ K$, pressure $p = 4.4\ dyn/cm^2$, opacity $\overline{\kappa}/\rho = 4.1 \cdot 10^{-4}\ cm^2/g$ from Eq. (20), specific heat $c_v = 9.6 \cdot 10^7\ erg/gK$, Stefan-Boltzmann constant $\sigma = 5.6 \cdot 10^{-5}\ erg/cm^2 s\ K^4$. It is seen that in timescales of a fraction of an hour the chromosphere would cool down to the boundary temperature if mechanical heating would suddenly stop.

3 Overview of the heating mechanisms

Tab. 2 summarizes the mechanisms which are thought to provide a steady supply of mechanical energy to balance the chromospheric and coronal losses

(Kuperus, Ionson & Spicer 1981, Wentzel 1981, Ulmschneider, Priest & Rosner 1991, Narain & Ulmschneider 1990, 1996). Here occasional transient and localized heating events like large flares are not considered, because they do not contribute appreciably to the persistent chromospheric and coronal heating. The term heating mechanism comprises three physical aspects, the *generation* of a carrier of mechanical energy, the *transport* of mechanical energy into the chromosphere and corona and the *dissipation* of this energy in these layers.

energy carrier	*dissipation mechanism*
hydrodynamic heating mechanisms	
acoustic waves, P<P_A	shock dissipation
pulsational waves, P>P_A	shock dissipation
magnetic heating mechanisms	
1. alternating current (AC) or wave mechanisms	
slow mode mhd waves, longitudinal mhd tube waves	shock dissipation
fast mode mhd waves	Landau damping
Alfvén waves (transverse, torsional)	mode-coupling resonance heating compressional viscous heating turbulent heating Landau damping
magnetoacoustic surface waves	mode-coupling phase-mixing resonant absorption
2. direct current (DC) mechanisms	
current sheets	reconnection (turbulent heating, wave heating)

Table 2. Heating mechanisms

Tab. 2 shows the various proposed energy carriers which can be classified into two main categories as *hydrodynamic* and *magnetic* heating mechanisms. Both the hydrodynamic and the magnetic mechanisms can be subdivided further by frequency. Acoustic waves are high frequency hydrodynamic fluctuations with periods $P < P_A$ (here P_A is the acoustic cut-off period, c.f.

Eq. (11)) and pulsational waves have periods $P > P_A$. The magnetic mechanisms are subdivided into high frequency wave- or AC(alternating current)-mechanisms and current sheet- or DC(direct current)-mechanisms where one has time variations of low frequency. Also in Tab. 2 the mode of dissipation of these mechanical energy carriers is indicated.

Ultimately the mechanical energy carriers derive their energy from the nuclear processes in the stellar core from where the energy is transported by radiation and convection to the stellar surface. In late-type stars the mechanical energy generation arises from the gas motions of the surface convection zones. These gas motions are largest in the regions of smallest density near the top boundary of the convection zone. Due to this, the mechanical energy carriers, particularly the waves, are generated in a narrow surface layer.

As the gas motions in the convection zone can be described by a common temporal and spatial turbulence spectrum consisting of a characteristic distribution from large to small cell size and from long to short time scales of the gas elements, it is clear that different parts of that spectrum are correlated with each other. We thus expect to find correlations between the various energy carriers owing to the common mode and region of generation.

4 Elementary heating processes

In the dissipation process, mechanical energy is converted into heat. That is, organized motion or potential energy is converted into random thermal motion. As will be shown below, an efficient conversion process is almost always associated with the generation of large variations of the physical variables over very small scales. For instance, it has been known for a long time that an efficient way to dissipate acoustic waves is the formation of shocks, where the physical variables abruptly vary over distances of a molecular mean free path.

Consider a typical acoustic or magnetohydrodynamic disturbance in the solar chromosphere with characteristic values, size $L = 200\ km$, temperature $\Delta T = 1000\ K$, velocity $\Delta v = 3\ km/s$ and magnetic field perturbation $\Delta B = 10\ G$. Using appropriate values for the thermal conductivity $\kappa_{th} = 10^5\ erg/cm\ s\ K$, viscosity $\eta_{vis} = 5 \cdot 10^{-4}\ dyn\ s/cm^2$ and electrical conductivity $\lambda_{el} = 2 \cdot 10^{10}\ s^{-1}$ we find for the ***thermal conductive heating rate*** $(erg\ cm^{-3}\ s^{-1})$

$$\Phi_C = \frac{d}{dz}\kappa_{th}\frac{dT}{dz} \approx \frac{\kappa_{th}\Delta T}{L^2} \approx 3 \cdot 10^{-7} \quad , \tag{8}$$

the *viscous heating rate* $(erg\ cm^{-3}\ s^{-1})$

$$\Phi_V = \eta_{vis}\left(\frac{dv}{dz}\right)^2 \approx \frac{\eta_{vis}\Delta v^2}{L^2} \approx 1 \cdot 10^{-7} \quad , \tag{9}$$

and the *Joule heating rate* $(erg\ cm^{-3}\ s^{-1})$

$$\Phi_J = \frac{j^2}{\lambda_{el}} = \frac{c_L^2}{16\pi^2\lambda_{el}} (\nabla \times B)^2 \approx \frac{c_L^2 \Delta B^2}{16\pi^2\lambda_{el} L^2} \approx 7 \cdot 10^{-5} \quad . \qquad (10)$$

Here j is the current density and c_L the light velocity. The three heating rates show that normally these processes are inadequate to balance the empirical chromospheric cooling rate of $10^{-1} erg\ cm^{-3}\ s^{-1}$ from the VAL81 model. Only when the length scale L is considerably decreased, can the heating rates be raised to acceptable levels. For acoustic waves as well as slow mode mhd- and longitudinal mhd tube waves, this is accomplished by shock formation. For magnetic cases, by the formation of current sheets.

5 Hydrodynamic heating mechanisms

There are two types of hydrodynamic mechanisms, *acoustic waves* and *pulsational waves*. Acoustic waves have periods less then the acoustic cut-off period

$$P_A = \frac{4\pi c_S}{\gamma g} \quad , \qquad (11)$$

where c_S is the sound speed, g the gravity and $\gamma = 5/3$ the ratio of specific heats. Pulsational waves have periods $P > P_A$. Typical values for the acoustic cut-off period for the Sun ($g = 2.74 \cdot 10^4\ cm/s^2$, $c_S = 7\ km/s$) are $P_A \approx 190\ s$ and for Arcturus ($g = 50\ cm/s^2$, $c_S = 6\ km/s$) $P_A \approx 1.5 \cdot 10^5\ s$.

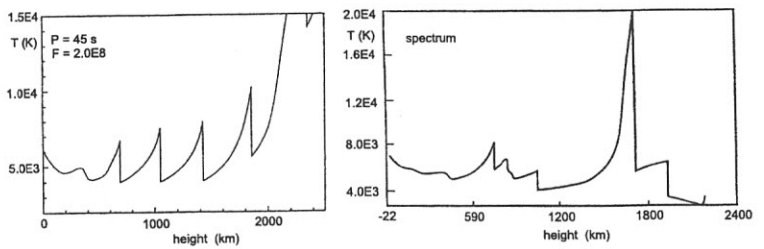

Fig. 1. Left panel: monochromatic, radiatively damped acoustic wave with period $P = 45\ s$ and initial energy flux $F_M = 2{\cdot}10^8\ erg\ cm^{-2}\ s^{-1}$. Right panel: propagating acoustic wave spectrum of the same initial energy.

For *late-type stars* of spectral type F to M, acoustic waves are generated by turbulent velocity fluctuations near the top boundary of the stellar convection zones. This process is discussed in detail in Sec. 8. Propagating down the steep density gradients of the outer stellar layers the acoustic waves suffer amplitude growth due to wave energy conservation. This amplitude growth

occurs despite of strong radiation damping. As the wave crests of large amplitude waves move faster than the wave troughs, shocks form by which the waves dissipate their energy.

Fig. 1 (left panel) shows a calculation of a monochromatic, radiatively damped acoustic wave of period $P = 45\ s$ and initial energy flux $F_M = 2{\cdot}10^8\ erg\ cm^{-2}\ s^{-1}$. It is seen that the wave grows from very small amplitude up to a point where sawtooth shocks form which attain a limiting strength. This limiting strength for a given star depends only on the wave period (larger periods give stronger shocks). Also shown in Fig. 1 (right panel) is a calculation with an acoustic spectrum. Here the wave energy likewise is dissipated by shocks.

In *early-type stars* of spectral type O to A, where the surface convection zones are absent, it is the intense radiation field of these stars which generates acoustic disturbances and amplifies them to strong shocks. This mechanism works as follows (c.f. Fig. 2). Consider a gas blob in the outer atmosphere of an early-type star. The line-opacity κ_ν as function of frequency ν of the gas in the blob at rest is shown dashed in Fig. 2. Also shown is the radiation intensity I_ν of the photospheric stellar radiation field which has an absorption line where κ_ν is large. If by chance the gas blob acquires a slight outward velocity, then its line-opacity κ_ν (drawn) becomes Doppler shifted towards the violet and photons from the violet side of the stellar absorption line will be absorbed in the blob, imparting their momentum and accelerate the blob even more (see Fig. 2). This results in a line-opacity κ_ν shifted even more out of the region of the photospheric absorption line etc. This process is called *radiative instability* and results in a powerful acceleration of the gas blobs which leads to the formation of strong shocks with x-ray emitting post-shock regions and intense local heating.

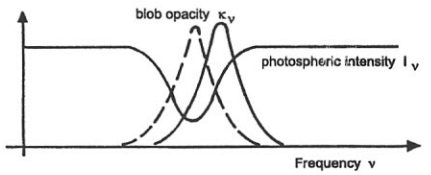

Fig. 2. Radiative instability for an accelerating gas blob in an intense radiation field.

The other hydrodynamic heating mechanism is by *pulsational waves*. Pulsational waves are prominent in Mira-star pulsations, but also in other late-type giants. These pulsations are generated by the *κ-mechanism*. The κ-mechanism (here κ refers to the opacity) functions similarly as the internal

combustion engine in motorcars (see Fig. 3). In the internal combustion engine a reactive gas mixture is compressed in a pulsational motion and is ignited at the moment of strongest compression, resulting in a violent decompression. The timing of the ignition ensures that the pulsational motion is amplified. In the κ-mechanism the opacity of stellar envelope material increases (due to the adiabatic temperature and pressure increase) when the star contracts in a pulsational motion. The opacity increase leads to an increased absorption of radiation energy and thus to a large heat input into the contracted envelope layers. The overheated envelope layers subsequently react by rapid expansion, thus driving the pulsation. These pulsational waves propagate to the outer stellar atmosphere where they form shocks.

This and related processes, in principle and possibly with different drivers (e.g. the $\epsilon-$*mechanism* where the nuclear energy generation is increased, see e.g. Kippenhahn & Weigert 1990), works also for nonradial oscillations. Any process which kicks on the basic pulsational and vibrational modes of the outer stellar envelope belongs to the category pulsational wave mechanisms. For the Sun the 3 min oscillation is such an example of a basic resonance which is generated by transient events produced in the convection zone. A systematic study of this heating mechanism for late-type stars is missing at the present time.

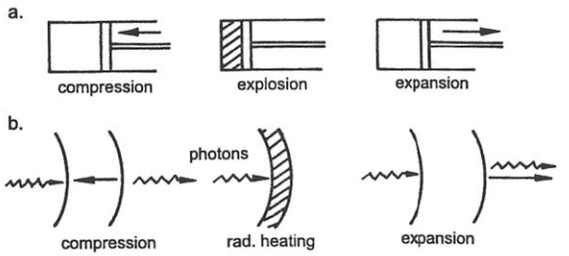

Fig. 3. a: Generation of pulsation by a gasoline engine, b: by the κ-mechanism.

6 Magnetic field structure

The magnetic fields of the Sun and their relation with the granulation and supergranulation cells, as well as the chromospheric network are discussed in other sections of this book. Reviews of the solar magnetic field structure have also been given by Mehltretter (1974), Zwaan (1978) and Stenflo (1978). It is found that the magnetic fields often appear in the shape of flux tubes both in the chromosphere and in the corona. At about 1500 km height the

individual flux tubes fill out the entire space and form the ***magnetic canopy.*** In the corona the field strength is $B \approx 10 - 100\ G$. At the surface of the Sun the field strength in an isolated flux tube of the chromospheric network is roughly $B \approx 1500\ G$. One has horizontal pressure balance

$$p_i + \frac{B^2}{8\pi} = p_e \quad , \tag{12}$$

where p_i is the gas pressure inside the flux tube and p_e the gas pressure in the non-magnetic region outside. At the solar surface at $z = 0$ one finds $p_e = 1.2 \cdot 10^5 dyn/cm^2$ in the VAL81 model. If the tube were empty, that is, $p_i = 0$, one would have $B = \sqrt{8\pi p_e} = 1740\ G$. This is called ***equipartition field strength.*** Actually the tube is not empty but has a gas pressure of about 1/4 to 1/5 of the outside pressure. Fig. 4 shows the three wave modes (Spruit 1981) which are thought to propagate along magnetic flux tubes. Longitudinal tube waves produce cross-sectional variations of the tube, they are essentially acoustic tube waves. The transverse and torsional Alfvén waves do not show a cross-sectional variation of the tube.

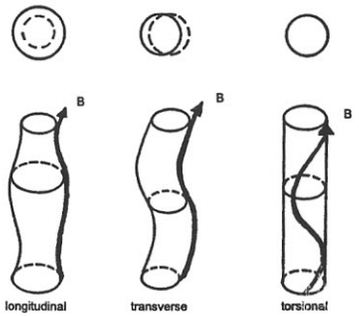

Fig. 4. The three possible wave modes in magnetic flux tubes.

7 Magnetic heating mechanisms

Consider a cylindrical magnetic flux tube of length $l_\parallel$ and diameter $l_\perp$, where the magnetic field B is along the axis of the tube. The convective gas motions outside the tube lead to magnetic field perturbations δB either in tangential or in radial direction. One then has $\delta B \approx B l_\perp / l_\parallel \approx B u \tau / l_\parallel$, where u is the velocity and τ the characteristic time of the convective flow. From this the energy density of the perturbation is (where $c_A = B/\sqrt{4\pi\rho}$ is the Alfvén speed)

$$E = \frac{\delta B^2}{4\pi} \approx \frac{B^2}{4\pi}\left(\frac{u}{l_\parallel}\right)^2 \tau^2 = \rho_o c_A^2 \left(\frac{u}{l_\parallel}\right)^2 \tau^2 \quad . \quad . \tag{13}$$

1. For slow tube motion ($\tau > l_\parallel / c_A$) one has a generated energy flux for the DC-mechanism

$$F_{DC} = E\frac{l_\parallel}{\tau} = \rho_o c_A^2 \frac{u^2}{l_\parallel}\tau, \quad . \tag{14}$$

2. for fast tube motion ($\tau < l_\parallel / c_A$), with an effective length $l_\parallel = c_A \tau$, one has a generated energy flux for the AC-mechanism

$$F_{AC} = \rho_o u^2 c_A. \quad . \tag{15}$$

A typical time scale is the Alfvén transit time t_A:

$$t_A = l_\parallel / c_A = l_\parallel \frac{\sqrt{4\pi\rho}}{B} \quad . \tag{16}$$

The magnetic waves are generated by *fast* ($t << t_A$) *turbulent velocity fluctuations* outside the tube. There velocity fluctuations are produced in the convection zone and affect the tube by compressional, transverse and torsional perturbations, but also by sudden events (see Sec. 7.8). Above the canopy the waves encounter a more or less *homogenous medium* and other wave modes are possible. *Fast* and *slow mode* magnetohydrodynamic (MHD) waves propagate there.

If the motions of the convection zone are *slow* ($t >> t_A$), then instead of waves, stressed magnetic structures are built up which contain a large amount of energy. Here often magnetic fields of opposite polarity are brought together and form current sheets. The energy of the stressed field is then released by *reconnection*, where the field lines break open and reconnect in such a way that the field geometry afterwards is simpler. These reconnection processes usually occur suddenly like in a *flare* where the magnetic field energy of a large spatial region is released in seconds. Smaller reconnection events are called *microflares*. The local release of energy generates waves in turn. However, same as for waves the ultimate *source* of the DC-heating mechanism is the *convection zone*.

Let us now list the main magnetic heating processes.

7.1 Mode-coupling

This mechanism is not a heating process by itself, but converts wave modes, which are difficult to dissipate by non-linear coupling into other modes, where the dissipation is more readily achieved. Typical cases are the conversion of transverse or torsional Alfvén waves into acoustic-like longitudinal tube waves which dissipate their energy by shock heating. Fig. 5 shows an example of such a process. It is seen that the magnetic tension force which is directed towards the center of curvature can be split into longitudinal and transverse

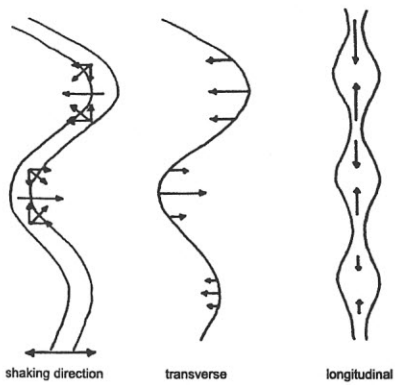

Fig. 5. Mode-coupling between transverse and longitudinal waves.

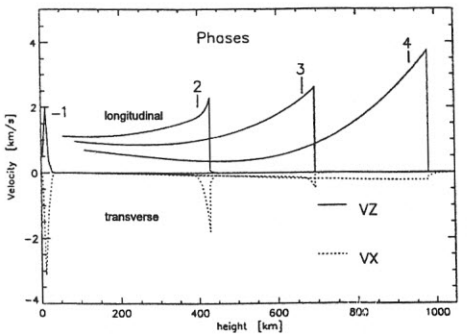

Fig. 6. Longitudinal wave pulse and shock generated by mode- coupling from an applied transverse wave pulse, after Zhugzhda et al. (1995).

components. The longitudinal force components act to compress the gas in the tube such that a longitudinal wave of twice the frequency is generated.

Mode-coupling is particularly efficient when the transverse waves are very stochastic in nature as is expected from observation (Muller et al. 1994) and from wave generation calculations (see Figs. 21 and 22 below). Fig. 6 (after Zhugzhda et al. 1995) shows the generation and development of a longitudinal shock wave pulse produced by mode-coupling from an applied transverse wave pulse. These calculations have to be taken with some caution because

of two reasons. First, the Zhugzhda et al. (1995) computations are performed with a one-dimensional time-dependent code using the thin tube approximation. There presently is an extensive not yet fully conclusive discussion in the literature about how to take into account for the swaying tube the back-reaction of the external fluid. Second, recent three-dimensional time-dependent work by Ziegler & Ulmschneider (1997) on swaying magnetic flux tubes in the solar atmosphere shows that there is extensive leakage of the transverse wave energy into the outside medium. Thus the true value of the longitudinal wave energy generation by mode-coupling is presently not well determined.

7.2 Resonance heating

Resonance heating occurs, when upon reflection of Alfvén waves at the two foot points of the coronal loops, one has constructive interference (see Fig. 7). For a given loop length $l_\parallel$ and Alfvén speed c_A, resonance occurs, when the wave period is $mP = 2l_\parallel/c_A$, m being a positive integer. Waves which fulfill the resonance condition are trapped and after many reflections are dissipated by Joule-, thermal conductive or viscous heating.

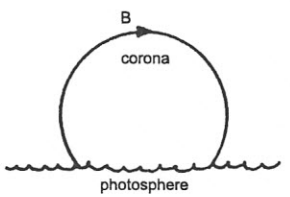

Fig. 7. Resonance heating in coronal loops.

7.3 Compressional viscous heating

Compressional viscous heating, recently proposed by Strauss (1991), is a very promising mechanism for coronal regions, where the gyro-frequency is much larger than the collision-frequency. Swaying an axial magnetic flux tube sideways with velocity $\mathbf{v}_\perp$ results in a transverse Alfvén wave which is incompressible ($\nabla \cdot \mathbf{v}_\perp = 0$) to first order. This is different for tubes with helicity, where one has $\nabla \cdot \mathbf{v}_\perp \approx \dot{\rho}/\rho$ (see Fig. 8). With an increase of the density, the magnetic field is compressed and the gyro-frequency increased. Gyrating around the field lines more quickly, the ions after colliding with each other, generate larger velocities in non-perpendicular directions as well, which constitutes the heating process.

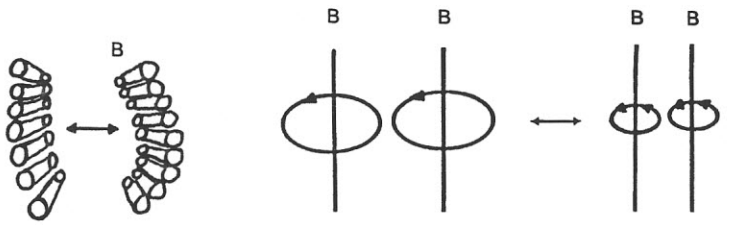

Fig. 8. Compressional viscous heating in helical fields.

7.4 Turbulent heating

In a turbulent flow field with high Reynolds number there are bubbles of all sizes. The energy usually is put into the largest bubbles. Because of the large inertial forces, the big bubbles are ripped apart into smaller bubbles, and these in turn into still smaller ones etc. This process is called turbulent cascade. A turbulent flow field can be described by three characteristic quantities, density ρ, bubble scale $l_k = 2\pi/k$, and the mean velocity u_k of such bubbles. k is the wavenumber. It is easily seen, that from these three quantities only one combination for a heating rate can be formed

$$\Phi_k = \rho \frac{u_k^3}{l_k} \quad \left[\frac{erg}{cm^3 s}\right] \quad . \tag{17}$$

If there are no other losses, like by radiation, all the energy which is put in at the largest bubbles must reappear in the smaller bubbles etc. Thus if $k1$, $k2, \cdots$ represents a series of smaller and smaller bubbles one must have $\Phi_{k1} = \Phi_{k2} = \cdots = \text{const}$. This implies

$$u_k \sim l_k^{1/3} \quad , \tag{18}$$

which is the *Kolmogorov law*. The range $l_{k1} \cdots l_{kn}$ of validity of this law is called the *inertial range*. Consider what happens if l_k becomes very small. From Eq. (9) one finds for the viscous heating rate, $\Phi_V = \eta_{vis}(du/dl)^2 \approx \eta_{vis} u_k^2/l_k^2 \approx \eta l_k^{-4/3}$, which goes to infinity for $l_k \to 0$. Thus at some small enough scale, viscous heating sets in and the inertial range ends. It is seen that turbulent heating lives from the formation of small scales. One can visualize the process as follows. Because of the continuous splitting of bubbles into smaller sizes, with the velocities decreasing much less rapidly, one eventually has close encounters of very small bubbles with large velocity differences where viscous heating dominates.

As the fluctuations generated in the turbulent convection zone produce acoustic and mhd waves it is of interest to deduce from the inertial range an estimate of the frequency range of the generated waves. If $k_0 \approx 2\pi/H$ is the

wavenumber of the scale where the energy is put into the turbulence, with H being the scale height, we have for the size l_k of the smallest bubble (where viscosity ends the cascade) $\eta_{vis} u_k^2/l_k^2 = \rho u_{k_0}^3/l_{k_0}$ and $u_k^3/l_k = u_{k_0}^3/l_{k_0}$. From this we obtain

$$l_k = \left(\frac{\eta_{vis} l_{k_0}^{1/3}}{\rho u_{k_0}} \right)^{3/4} . \tag{19}$$

With $l_{k_0} = H = 150\ km$, $u_{k_0} = 1\ km/s$, $\rho = 3 \cdot 10^{-7}\ g/cm^3$, $\eta_{vis} = 5 \cdot 10^{-4}\ dyn\ s/cm^2$, one finds $l_k = 2.9\ cm$ as well as $u_k = 290\ cm/s$ and derives a maximum frequency of $\nu_k = u_k/l_k = 100\ Hz$ or a period of $P = 1/100\ s$. This estimate is somewhat idealized as small bubbles become transparent to radiation. In this case the temperature excess, which drives the convection, is exchanged directly via radiation. Thus it is expected that the optical depth limits the bubble size. Assuming that the smallest bubble has an optical depth of $\tau = l_k \overline{\kappa} = 0.1$, where

$$\frac{\overline{\kappa}}{\rho} = 1.38 \cdot 10^{-23} p^{0.738} T^5 \quad \mathrm{cm}^2/\mathrm{g} \quad , \tag{20}$$

is the gray H^- opacity, $T = 8320\ K$ the temperature and $p = 1.8 \cdot 10^5\ dyn/cm^2$ the gas pressure, one finds $l_k = 6.3 \cdot 10^4\ cm$, $u_k = 1.6 \cdot 10^4\ cm/s$, $\nu_k = 0.25\ Hz$ and $P = 3.9\ s$ for the smallest bubble.

So far we have discussed turbulent heating in a non-magnetic environment. When there is a magnetic flux tube one has to take into account the tube geometry, the frozen-in condition and the wave modes. Fig. 9 shows how the turbulent dissipation of a torsional Alfvén wave is pictured (after Heyvaerts & Priest 1983, Hollweg 1983). Shearing motions in azimuthal direction generate closed magnetic loops (similarly to the growth of Helmholtz-Kelvin-type instabilities) over the tube-cross-section, which decay into smaller tubes etc. and are ultimately dissipated by reconnection.

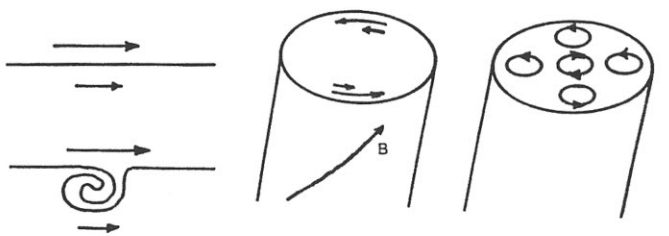

Fig. 9. Turbulent heating in magnetic flux tubes.

7.5 Landau damping

Landau damping occurs at coronal heights, where the collision rate becomes small. As Chen (1974) has explained, this process is analogous to surfing on ocean waves (see Fig. 10). When surfing, a surfboard rider launches himself in propagation direction into the steepening part of an incoming wave and gets further accelerated by this wave. In Landau damping, the propagating wave accelerates gas particles which, due to their particle distribution function, happen to have similar direction and speed as the wave. Because a distribution function normally has many more slower particles than faster ones, the wave looses energy to accelerate the slower particles. This gained energy is eventually shared with other particles in the process to reestablish the distribution function, which constitutes the heating mechanism.

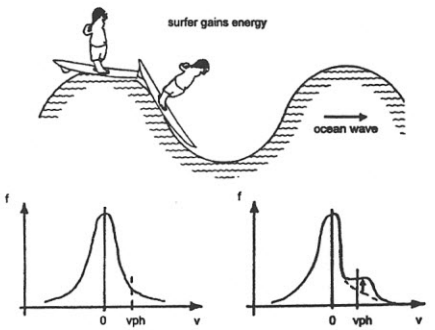

Fig. 10. Landau damping and the analogy to surfing.

7.6 Resonant absorption

In the process of resonant absorption one considers magnetoacoustic surface waves in a magnetic field **B** which points in z-direction, and varies from $\mathbf{B_1}$ to $\mathbf{B_2}$ in x-direction (see Fig. 11, panel a). The surface wave, with its field perturbation $\delta B = B_x'$ in x-direction, has a phase speed $v_{ph} = ((B_1^2 + B_2^2)/(4\pi(\rho_1 + \rho_2))^{1/2}$, such that at an intermediate position x_o, the phase speed becomes equal to the local Alfvén speed $c_{Ao} = B(x_o)/\sqrt{4\pi\rho(x_o)}$. In panel b of Fig. 11 consider the wave fronts of the peak (drawn) and trough (dotted) of a surface wave. Because to the right of x_o, the Alfvén speed is

larger and to the left smaller, the wave fronts at a later time get tilted, relative to the phase, propagating with speed c_{Ao} (see panel c). At a still later time (panel d) the wave fronts get tilted even further and approach each other closely at the position x_o. This leads to small scales and intense heating by reconnection at that field line.

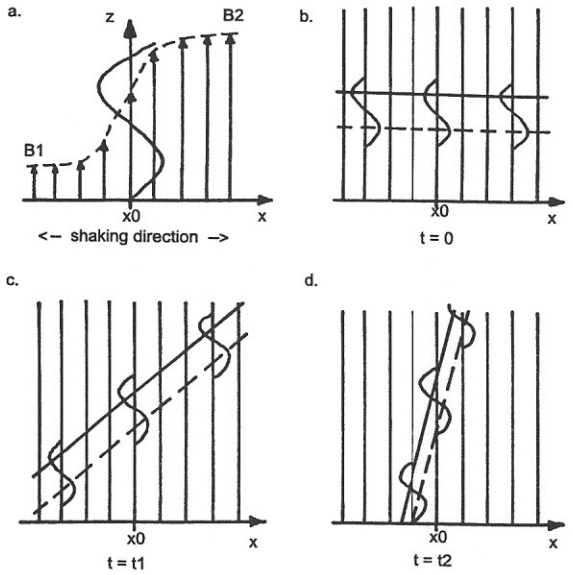

Fig. 11. Resonant absorption. In a field pointing in z-direction, where the field strength varies in x-direction. a: resonant absorption of a surface wave (shaking in x-direction), b: wave fronts at time $t = 0$, and c:, d: at later times t_1, t_2.

7.7 Phase-mixing

For phase-mixing (c.f. Fig. 12) one considers a magnetic field geometry similar to that in Fig. 11, however, the field perturbation $\delta B = B'_y$ of the wave is now in y-direction, perpendicular to the x- and z-directions. As the Alfvén speeds of two closely adjacent regions x_1 and x_2 are different, it is seen that after propagating some distance Δz, the fields $B'_y(x_1)$ and $B'_y(x_2)$ will be very different, leading to a current sheet and strong dissipation. Here again it is the appearance of small scale structures which lead to dissipation.

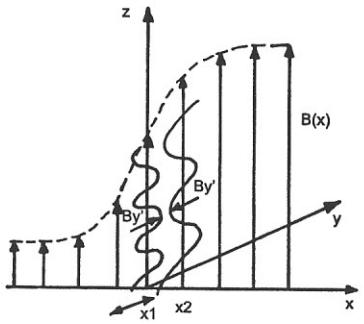

Fig. 12. Phase-mixing of a surface wave (shaking in y-direction).

7.8 Reconnection in current sheets

As example of the DC heating mechanisms, Fig. 13, after Parker (1991), shows how slow foot point motions caused by the convection zone at both legs of a coronal loop, starting from a minimum energy axial field state (left panel), will build up a tangled and braided field configuration of high energy (right panel). Note that in Fig. 13 the two legs of the tube (z = 0, z = L) are drawn such that they appear at the bottom and top. As the foot point motions perpetually increase the energy buildup, the system tries increasingly hard to return to a lower energy state. Because of the hopelessly complicated tangling this can only be achieved via reconnection. At many locations in the web of field lines, oppositely directed fields occur, giving rise to local current sheets, which by reconnection (in the form of microflares) release the magnetic field energy. The energy is dissipated both directly and via the generation of waves and turbulence. Note that similarly to the wave mechanisms, reconnection happens in small scale regions. These reconnective events of different magnitude have been observed on the Sun by Brueckner & Bartoe (1983) as sudden velocity shifts in the C IV ($T \approx 10^5\ K$) transition layer line with velocities of 250 km/s and even 400 km/s. The authors have termed these phenomena turbulent events and high velocity jets, respectively.

The question, whether microflares is a significant coronal heating mechanism and what its importance is as compared to wave heating (DC– versus AC–heating), has recently been studied by Wood, Linsky & Ayres (1996) by observing CIV and Si IV transition layer lines (see Fig. 14). They found that the total line profile can be explained as a combination of a very broad profile, attributed to microflares, and a narrow profile, attributed the wave heating. A careful study of observations of this type, particularly with respect to the three stellar parameters T_{eff}, gravity and rotation, will allow to make

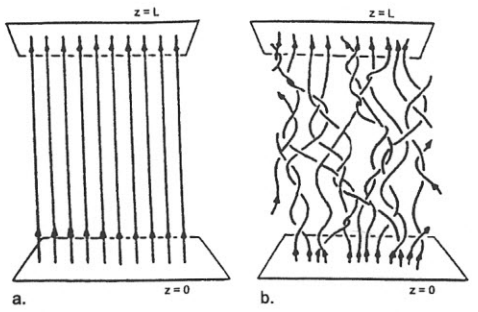

Fig. 13. a: Magnetic fields in coronal loops, initial axial field (left), b: tangled fields after considerable foot point motions (right), after Parker (1991).

great progress in the identification of the individual heating processes and generally in the understanding of coronal heating as a function of the basic parameters of the underlying stars.

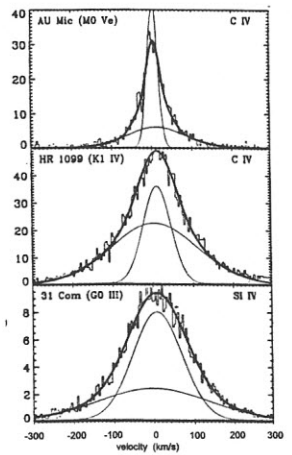

Fig. 14. Surface fluxes in transition layer lines (in $10^4\ erg\ cm^{-2}\ s^{-1}\ A^{-1}$) of giants and main sequence stars, after Wood et al. (1996).

Another example of current sheet formation and heating is seen in Fig. 15, after Priest (1991). It shows an arcade system, which by slow motion is

laterally compressed and develops a current sheet. Here oppositely directed fields reconnect. Similar systems of approaching magnetic elements of opposite polarity and large scale field annihilation are thought to be responsible for the heating of X-ray bright points.

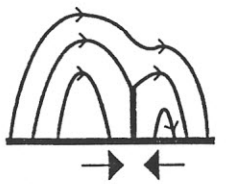

Fig. 15. Current sheets in arcade systems, after Priest (1991).

8 Acoustic energy generation

8.1 The process of quadrupole sound generation

Typically in stellar convection zones, sound is generated by pressure and density fluctuations produced by Reynolds stresses (Fig. 16). Such sound generation by free turbulence, called *quadrupole sound generation*, is the most efficient way to generate sound even in terrestrial situations, when mass injections and rigid vibrating surfaces are absent. Chopped mass injection like in a rotating perforated disk siren is the most efficient way to produce sound and is termed *monopole sound generation*, while vibrating surfaces like in a tuning fork leads to the less efficient *dipole sound generation*.

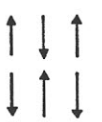

Fig. 16. Reynolds stresses.

Using the linearized continuity equation and the equation of motion one has

$$\frac{\partial \rho'}{\partial t} + \nabla \cdot \rho_0 \mathbf{v} = 0 \quad , \tag{21}$$

$$\frac{\partial \rho_0 \mathbf{v}}{\partial t} + c_S^2 \nabla \rho' = -\nabla \cdot \rho_0 \mathbf{v}\mathbf{v} \quad . \tag{22}$$

Here we retain the Reynolds stress term $\rho_0 \mathbf{v}\mathbf{v}$ which usually in the linearized equations is *neglected* as normally (21), (22) contain only first order terms. We expect therefore that this source term is very small. Operating with $\partial/\partial t$ on (21) and with $-\nabla\cdot$ on (22) and adding, a wave equation with a source term is obtained

$$\left(\frac{\partial^2}{\partial t^2} - c_S^2 \nabla^2\right) \rho' = \nabla\nabla : \rho_0 \mathbf{v}\mathbf{v} \quad . \tag{23}$$

In a stellar convection zone the velocity $\mathbf{v}$ in the source term is given by the convective velocity u and because the flow time scales are much slower one has

$$\frac{\partial}{\partial t} \rightarrow \frac{u}{c_S} \frac{\partial}{\partial t} \quad . \tag{24}$$

With this and with $\nabla \sim \frac{1}{c_S} \frac{\partial}{\partial t}$ at the RHS we find from Eq. (23)

$$\rho' \approx \rho_0 \frac{u^4}{c_S^4} \quad . \tag{25}$$

The acoustic energy flux F_M is twice the kinetic energy density (because of equipartition of kinetic and potential energy) times the sound speed:

$$F_M = \rho_0 v^2 c_S \quad . \tag{26}$$

Using the amplitude relations for sound waves

$$\frac{\rho'}{\rho_o} = \frac{v}{c_S} = \frac{p'}{\gamma p_o} \quad , \tag{27}$$

one finds for the acoustic flux by *quadrupole sound generation:*

$$F_M^{quad} = \frac{1}{\rho_0} c_S^3 \rho'^2 = \rho_0 \frac{u^8}{{c_S}^5} \quad . \tag{28}$$

Considering a Kolmogorov turbulence spectrum (like our Eq. (31), below), Lighthill has derived from (28) the expression

$$F_M = \int 38 \frac{\rho_0 u^8}{c_S^5 H} dz \quad , \tag{29}$$

called *Lighthill- or Lighthill-Proudmann formula*, where H is the scale height. Fig. 17 taken from Goldstein (1976) shows how well Lighthill's u^8–formula is observed to work in terrestrial applications. Here gas from jet engines is directed against a wire mesh, behind which turbulent flows develop. As there is neither mass injection nor a vibrating surface, one has quadrupole sound generation.

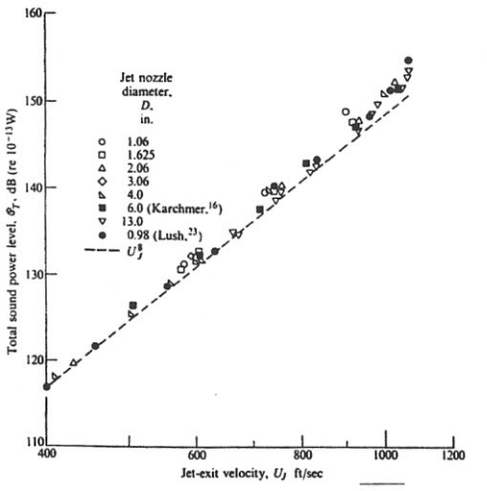

Fig. 17. Noise from jet engines, after Goldstein (1976).

8.2 Acoustic flux computations for stars

Quadrupole sound generation from turbulence was originally developed by Lighthill (1952, 1954) as well as Proudman (1952) and was further extended by Stein (1967, 1968) to stellar convection zones. The Lighthill-Stein theory has been rediscussed in detail by Musielak et al. (1994). These authors found that the stellar turbulence is best represented by a Kolmogorov-type energy spectrum (see Eqs. (31) to (34), below).

To calculate acoustic fluxes of the Sun and of stars *three parameters have to be specified*: T_{eff}, g and the mixing-length parameter α, where α is the ratio of the mixing-length to the scale height. Typically one has $\alpha \approx 1.5$ to 2.0. These three parameters uniquely specify a *convection zone model.* This model provides ρ_0, u, c_S and H versus z and allows to calculate the acoustic fluxes F_M using the described methods. Acoustic fluxes as well as acoustic energy spectra computed this way for a large number of late-type stars in the HR-diagram (after Ulmschneider, Theurer & Musielak 1996) are shown in Figs. 18 and 19. These authors find that the total acoustic fluxes using the very elaborate Lighthill-Stein theory are fairly close to the values given by the simple Lighthill formula (see dotted values in Fig. 18). This fact is due to the use of the Kolmogorov spectrum in both methods.

While in terrestrial situations, monopole, dipole and quadrupole sound generation is a sequence of progressively less important ways to produce

acoustic waves, this is different in stellar situations, where external mass injections and rigid surfaces are absent. Here quadrupole sound generation is largest and, except for late-type dwarf stars, even dominant. The acoustic

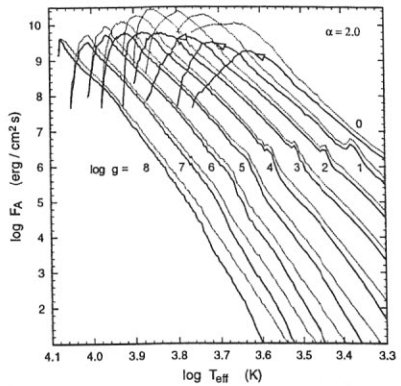

Fig. 18. Acoustic fluxes F_M for stars versus T_{eff} for given $\log g$ and $\alpha = 2.0$.

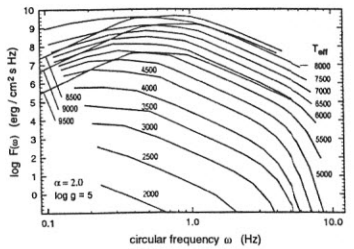

Fig. 19. Acoustic spectra $dF_M(\omega)/d\omega$ for stars versus circular frequency ω for given T_{eff} and $\alpha = 2.0$, for $\log g = 5$.

spectra extend roughly over the range $\omega_A < \omega < 20\omega_A$ (see Fig. 19), where $\omega_A = 2\pi/P_A = \gamma g/2c_S$ is the acoustic cut-off frequency and P_A the acoustic cut-off period. $\omega = 2\pi\nu = 2\pi/P$ is the circular frequency and P the wave period. For the Sun the acoustic spectrum has a maximum at a period

$$P_{max} \approx \frac{P_A}{4} \approx 60\ s \quad . \tag{30}$$

At this point it is interesting to show an application of the acoustic wave

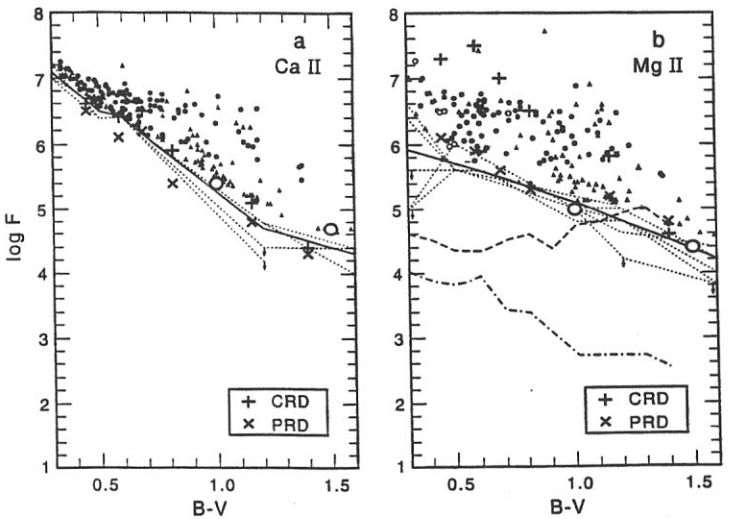

Fig. 20. Theoretical and empirical chromospheric emission fluxes in the Ca II and Mg II lines versus colour for late-type stars, after Buchholz et al. (1997).

generation computations which allowed to identify acoustic waves as the main heating mechanism for magnetic field free regions in late-type stars. Fig. 20 shows the chromospheric emission flux in the Ca II H+K and the Mg II h+k lines of late-type stars versus the color index B-V after Buchholz, Ulmschneider & Cuntz (1997). Here the dots represent main-sequence and the triangles giant stars. It is seen that the stars have a minimum emission (given by the drawn empirical line, called *basal flux line*) which is interpreted as due to pure acoustically heated chromospheres. Dots and triangles above this line represent stars which have additional magnetic heating, correlated with rotation. Also shown are simulations (x's for main-sequence and circles for giant stars) obtained from theoretical chromosphere model calculations based on the generated acoustic wave fluxes. The nice agreement of the theoretical and empirical (basal) emission fluxes for a wide range of stars with different T_{eff} (equivalent to B-V) and gravity shows the validity of acoustic heating. The conclusion, that acoustic heating is the main mechanism for magnetic field free regions of stars, could not have been drawn from solar observations alone, as here the magnetic and hydrodynamic heating mechanisms are very

difficult to disentangle. Varying the T_{eff} and gravity dependences of the different heating mechanisms allows to identify the important mechanisms using stellar observations.

9 Magnetic energy generation

The radiative emission of the solar chromosphere is particularly concentrated in the network region surrounding supergranulation cells. Here strong vertically directed magnetic flux tubes have been collected by the convective granular and supergranular flows and were strengthened by the convective collapse. The turbulent non-magnetic environment outside these flux tubes strangles and displaces the magnetic tubes which leads to the generation of longitudinal and transverse mhd waves. These tubes, moreover, are thought to occupy the centers of cyclonic downflow channels where turbulent motions give rise to torsional perturbations of the tubes which lead to the generation of torsional waves. Thus all three wave types, longitudinal, transverse and torsional modes are generated by the turbulent convection zone.

Both solar observations and theoretical convection zone simulations show that the turbulent energy spectrum is reasonably well described by a Kolmogorov type law. As shown by Musielak et al. (1994) the turbulence in the solar convection zone can very likely be represented by an extended Kolmogorov spectrum $E(k)$ with a modified Gaussian frequency factor $\Delta(\frac{\omega}{ku_k})$. The extended Kolmogorov spectrum (which describes the energy distribution among the different spatial scales k) is given by

$$E(k) = \begin{cases} 0 & : \ 0 < k < 0.2k_t \\ a\frac{u_t^2}{k_t}\left(\frac{k}{k_t}\right) & : \ 0.2k_t \le k < k_t \\ a\frac{u_t^2}{k_t}\left(\frac{k}{k_t}\right)^{-5/3} & : \ k_t \le k \le k_d \end{cases} , \tag{31}$$

where the factor $a = 0.758$ is determined from the normalization condition

$$\int_0^\infty E(k)dk = \frac{3}{2}u_t^2 \quad . \tag{32}$$

The modified Gaussian frequency factor (describing the temporal behaviour of the turbulence) is given by

$$\Delta\left(\frac{\omega}{ku_k}\right) = \frac{4}{\sqrt{\pi}}\frac{\omega^2}{|ku_k|^3}e^{-(\frac{\omega}{ku_k})^2} \quad , \tag{33}$$

where ω is the circular frequency and u_k the velocity of bubbles of scale k. u_k is computed from

$$u_k = \left[\int_k^{2k} E(k')dk'\right]^{1/2} \quad . \tag{34}$$

Here $k_t = 2\pi/H$ (H being the scale height) is the characteristic scale where the main energy input occurs. u_t is the root mean square velocity in one spatial direction (see Eq. (36) below).

Assume that at a given height z, the horizontal turbulent velocity fluctuation in one spatial direction can be described by a large number of ($N \approx 100$) superposed partial waves of given frequencies ω_n

$$v_x(z,t) = \sum_{n=1}^{N} u_n \sin(\omega_n t + \varphi_n) \ , \tag{35}$$

as function of time t. Here $\varphi_n = 2\pi r_n$ is an arbitrary but constant phase angle and r_n a random number in the interval [0, 1]. The amplitude of the partial waves u_n is then determined from the normalization condition of the assumed turbulent energy spectrum:

$$\frac{3}{2}u_t^2 = \frac{3}{2}\overline{v_x^2} = \frac{3}{4}\sum_{n=1}^{N}u_n^2 = \int_0^\infty d\omega \int_0^\infty dk \ E(k)\Delta\left(\frac{\omega}{ku_k}\right) = \sum_{n=1}^{N}E'(\omega_n)\Delta\omega \ . \tag{36}$$

To compute transverse tube wave fluxes we let the external velocity fluctuations $v_x(z,t)$ shake the tube, while for longitudinal tube waves we let the external turbulent pressure fluctuations p_{turb} work on the tube. For a thin magnetic flux tube sticking in a convection zone, the pressure balance of Eq. (12) is modified and now given by

$$p + \frac{B^2}{8\pi} = p_e + p_{turb} \quad , \tag{37}$$

where

$$p_{turb} = \rho_e\left(v_x^2(\mathbf{r},t) + v_y^2(\mathbf{r},t) + v_z^2(\mathbf{r},t)\right) \quad . \tag{38}$$

Upon time averaging one finds for homogeneous isotropic turbulence

$$p_0 + \frac{B_0^2}{8\pi} = p_e + 3\rho_e u_t^2 \quad , \tag{39}$$

where p_0 is the average internal gas pressure and B_0 the average magnetic field strength. This equation shows that when one adds a turbulent flow outside the magnetic flux tube, then the mean external pressure is increased. This is due to the fact that in Eqs. (37), (38) the external turbulent pressure is a quantity which cannot be negative and thus must fluctuate around an average positive value. This additional turbulent pressure is small, typically one finds $\overline{p_{turb}} = 6 \cdot 10^{-2}p_e$.

Subtracting the averaged equation from Eq. (37) one obtains a perturbation equation

$$p' + \frac{B_0 B'}{4\pi} = p_{turb} - 3\rho_e u_t^2 = p'_{turb} \quad , \tag{40}$$

where $p' = p - p_0$ is the internal gas pressure fluctuation and $B' = B - B_0$ the magnetic field strength perturbation. In a thin tube p' and B' are related and one finds

$$p' = \frac{\beta}{1+\beta}\, p'_{turb} \quad , \tag{41}$$

where $\beta = 8\pi p_0/B_0^2$ is the plasma β. Making use of the amplitude relations for longitudinal tube waves, and the tube speed $c_T = c_S c_A/\sqrt{c_S^2 + c_A^2}$ one finds for the internal longitudinal velocity fluctuations

$$v_{\parallel} = \frac{c_S^2}{c_T}\frac{p'}{\gamma p_0} = \frac{\beta}{1+\beta}\frac{p'_{turb}}{\rho_0 c_T} = \frac{\beta}{1+\beta}\frac{3\rho_e(v_x^2 - u_t^2)}{\rho_0 c_T} \quad . \tag{42}$$

The velocity fluctuations v_x and $v_{\parallel}$ constitute the boundary conditions for a time-dependent one-dimensional magnetohydrodynamic wave code with which the transverse and longitudinal tube wave fluxes (Huang, Musielak & Ulmschneider 1995, Ulmschneider & Musielak 1997) can be computed employing the expressions

$$F_{trans} = -\frac{B}{4\pi} B_x v_x \quad , \tag{43}$$

and

$$F_{long} = \left(1 + \frac{5}{4}\beta\right) v_{\parallel} p' \quad . \tag{44}$$

Note that the magnetic field perturbation B_x and the pressure perturbation p' are automatically evaluated (including their phase-shifts against the velocity fluctuations) in the wave code by the mhd equations, once the time-dependent velocity boundary conditions are specified.

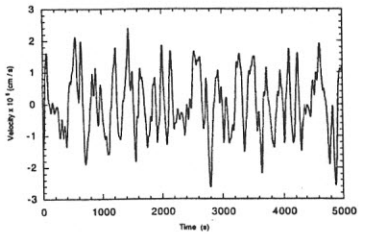

Fig. 21. Fluctuating turbulent velocity v_x as function of time for an extended Kolmogorov energy spectrum with a modified Gaussian frequency factor for an assumed rms convective velocity $u_t = 1 km/s$.

Fig. 21 shows the fluctuating horizontal velocity v_x computed using Eq. (35) for a prescribed rms turbulent velocity of $u_t = 1\ km/s$. It is seen that

due to the many partial waves, v_x is very stochastic in nature. u_t is a typical mean excitation velocity which is about one third of the maximum convective velocity obtained from a convection zone code for the Sun using a mixing-length parameter $\alpha = 2$. Fig. 21 shows that occasionally large velocity spikes occur which can approach 3 km/s, which is in good agreement with observations. The instantaneous and time-averaged transverse and longitudinal

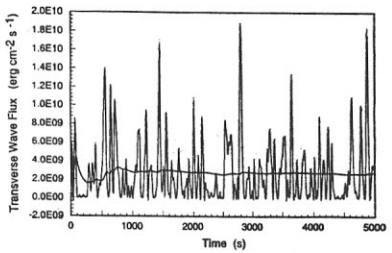

Fig. 22. Instant and time-averaged transverse tube wave energy fluxes versus time.

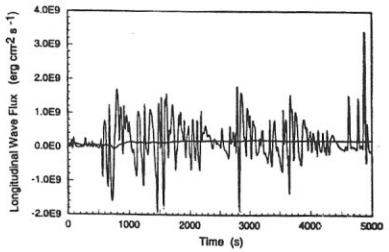

Fig. 23. Instant and time-averaged longitudinal tube wave energy fluxes versus time.

wave energy fluxes resulting from these excitations are shown in Figs. 22 and 23. From several computations using mean excitation velocities $u_t = 1.0$ to 1.5 km/s and varying the shaking height from -150 to +150 km height in the solar atmosphere one finds that the longitudinal tube wave fluxes F_{long} are of the order of $3 \cdot 10^8 erg\ cm^{-2}\ s^{-1}$ and the transverse tube wave fluxes are about a factor of 20 larger. Figs. 24 show the computed mhd tube wave energy spectra. It is seen that these spectra are dominated in their frequency behaviour by the Kolmogorov input spectrum.

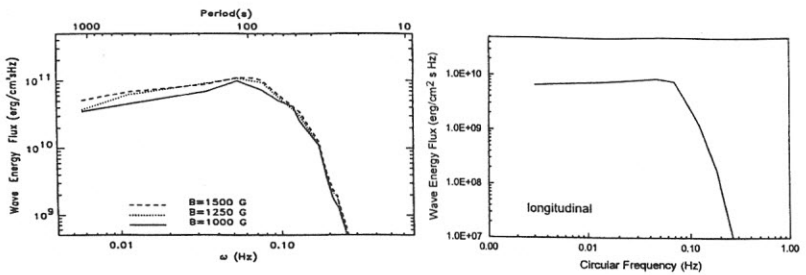

Fig. 24. Left: Fourier spectrum of the transverse, right: of the longitudinal energy flux.

10 Conclusions

Probably all nondegenerate stars have chromospheres and coronae. These hot outer layers are physically completely dependent on the properties of the underlying star and it is our ultimate aim to elucidate this physical dependence. Chromospheres and coronae owe their existence to mechanical heating. There are *hydrodynamical–* and *magnetic heating mechanisms*, each of which, on basis of the frequency of fluctuations, can by further classified into subcategories (acoustic– and pulsational waves as well as AC– and DC–mechanisms).

Rapid fluctuations generated by the turbulence in the convection zones lead to acoustic waves and to mhd waves (AC–mechanisms), slow fluctuations to pulsational waves and to stressed fields with current sheets (DC–mechanisms). Acoustic and mhd wave generation rates can presently be computed on basis of convection zone models and the (Kolmogorov–type) energy spectrum of the turbulence for a large number of stars.

Nonmagnetic chromospheric regions of late-type stars appear to be heated by shock dissipation of *acoustic waves*. For slowly rotating stars, which have weak or no magnetic fields, acoustic waves are the dominant chromospheric heating mechanism.

Except for F-stars and giants, the chromospheric heating of rapidly rotating late-type stars is dominated by *magnetic heating*. This heating very likely is by acoustic-like longitudinal mhd tube waves in the lower chromosphere up to the transition layer, and by Alfvén waves in the transition layer and corona. But these higher layers and the corona are also efficiently heated by DC–mechanisms (microflares). Note that microflares lead to both direct dissipation and wave generation.

Which of the various proposed mechanisms is the prime candidate for the dissipation of Alfvén waves is presently not well understood. This is also true for the question in what situation DC– or AC–heating is more important.

Here mhd modeling using the complete fluctuation spectrum of the convection zone and more solar and stellar observations will bring the answer.

References

Brueckner G.E., Bartoe J.D.F.: 1983, ApJ 272, 329
Buchholz B., Ulmschneider P., Cuntz, M.: 1997, ApJ, in press
Chen 1974, *Introduction to Plasma Physics*, Plenum Press, New York
Goldstein M.E.: 1976, *Aeroacoustics*, Mc Graw Hill, New York
Heyvaerts J., Priest E.R.: 1983, A&A 117, 220
Hollweg J.V.: 1983, in *Solar Wind V*, M. Neugebauer Ed., NASA CP-2280, p. 5
Huang P., Musielak, Z.E., Ulmschneider P., 1995, A&A 279, 579
Kippenhahn R., Weigert A.: 1990, *Stellar Structure and Evolution*, Springer, Berlin
Kuperus, Ionson, Spicer: 1981, Ann. Rev. Astr. Ap. 19, 7
Lighthill M.J.: 1952, Proc. Roy. Soc. London A211, 564
Lighthill M.J.: 1954, Proc. Roy. Soc. London A222, 1
Linsky J.L., 1985, Solar Phys. 100, 333
Mehltretter, P.: 1974, Solar Phys. 38, 43
Muller R., Roudier Th., Vigneau J., Auffret H.: 1994, A&A 283, 232
Musielak Z.E., Rosner R., Stein, R.F., Ulmschneider P., 1994, ApJ 423, 474
Narain, U. & Ulmschneider, P.: 1990, Space Sci. Rev. 54, 377
Narain, U. & Ulmschneider, P.: 1996, Space Sci. Rev. 75, 453
Parker E.N.: 1991, in *Mechanisms of Chromospheric and Coronal Heating*, Springer, Berlin, p. 615
Priest E.R.: 1991, in *Mechanisms of Chromospheric and Coronal Heating*, Springer, Berlin, p. 520
Proudmann I.: 1952, Proc. Roy. Soc. London A214, 119
Spruit, H.: 1981, A&A 98, 155; 102, 129
Stein R.F.: 1967, Solar Phys. 2, 385
Stein R.F.: 1968, Ap.J. 154, 297
Stenflo: 1978, Rep. Progr. Phys. 41, 865
Strauss H.R.: 1991, Geophys. Res. Let. 18, 77
Ulmschneider P., Musielak Z.E. 1997, A&A, in press
Ulmschneider P., Theurer J., Musielak Z.E.: 1996, A&A 315, 212
Ulmschneider, P., Priest E.R., Rosner R.: 1991, *Mechanisms of Chromospheric and Coronal Heating*, Springer, Berlin
Ulmschneider P., 1991, in *Mechanisms of Chromospheric and Coronal Heating*, Springer, Berlin, p. 328
Vaiana G.S. et al.: 1981, ApJ 245, 163
Vernazza J.E., Avrett E.H., Loeser R., 1981, ApJ Suppl 45, 635
Wentzel: 1981, *The Sun as a Star*, NASA-CNRS Series
Wood B.E., Linsky J.L., Ayres T.R.: 1996, ApJ 478, 745
Zhugzhda Y., Bromm V., Ulmschneider P.: 1995, A&A 300, 302
Ziegler U., Ulmschneider P.: 1997, A&A, in press
Zwaan, C.: 1978, Solar Phys. 60, 213